DIN
GMA

Quaderni di ricerca

Ottava giornata di studio
Ettore Funaioli

18 luglio 2014

A cura di
Umberto Meneghetti, Alberto Maggiore e Vincenzo Parenti Castelli

SOCIETÀ EDITRICE ESCULAPIO

AlmaDL

Quaderni del **DIN – GMA**

Atti di giornate di studio – 8

A cura di:
U. Meneghetti , A. Maggiore , V. Parenti Castelli

Coordinatore di redazione:
Alessandro Zanarini

DIN
Dipartimento di Ingegneria Industriale
http://www.ingegneriaindustriale.unibo.it

GMA
Gruppo di Meccanica Applicata
http://wpage.unina.it/dellaval/GMA/GMA_homeold.htm

Accademia delle Scienze dell'Istituto di Bologna
http://www.accademiascienzebologna.it/AccademiaScienze/default.htm

Ottava giornata di studio Ettore Funaioli

18 luglio 2014

A cura di:
Umberto Meneghetti, Alberto Maggiore e Vincenzo Parenti Castelli

Ottava giornata di studio Ettore Funaioli – 18 luglio 2014 / A cura di Umberto Meneghetti, Alberto Maggiore, Vincenzo Parenti Castelli
Bologna: 2015 – pp. 282; 17 cm

ISBN 978-88-7488-871-9

Versione elettronica disponibile alla pagina
http://amsacta.unibo.it/4301/

Stampa a richiesta eseguita da:

40131 Bologna – Via U. Terracini 30 – Tel. 051- 6340113 – Fax 051- 6341136
www.editrice-esculapio.com

INDICE

Prefazione

M. Peroni, F. Leali, A. O. Andrisano, M. Forte 1
Archetype-based design of mechanical transmissions

F. Montanari, M. Cocconcelli, L. Orazi, R. Rubini 11
Ottimizzazione dei percorsi CNC per lavorazioni laser di superfici free form

A. O. Andrisano, F. Balugani, G. Berselli, M. Gadaleta, M. Pellicciari, A. Vergnano 27
Progettazione di traiettorie energeticamente efficienti in servomeccanismi per macchine automatiche

E. Prati, A. Tasora, S. Longarini, V. Pollastri 37
Studio dell'usura e del momento resistente di anelli di tenuta in elastomero al variare della rugosità dell'albero

C. Mazzotti, M. Troncossi, V. Parenti Castelli 47
Functional design of a new finger exoskeleton based on a Stephenson type mechanism

M. Conconi, N. Sancisi, M. Forlani, V. Parenti Castelli 59
Measure and analysis of motion and muscle forces at the human knee during dynamic motion tasks

A. Martini, M. Troncossi, M. Carricato, A. Rivola 67
Gravity compensation of the orthoglide 5-axis parallel kinematics machine

G. Scirè Mammano, E. Dragoni 75
Modelling and validation of a continuous rotary motor combining shape memory wires and overrunning clutches

A. O. Andrisano, L. I. Manevitch, F. Pellicano, M. Strozzi 97
Nonlinear oscillations and energy localization in carbon nanotubes

N. Golinelli, A. Spaggiari 107
Design of a novel magnetorheological damper with internal pressure control

A. Carminelli, G. Catania 119
Chatter stability analysis of high speed machining by means of spectral decomposition modeling

M. Cocconcelli, M. Troncossi, A. Agazzi, E. Mucchi, R. Rubini, A. Rivola, G. Dalpiaz 135
Improvement of the dynamic behaviour of a test bed driveline by numerical and experimental investigations

M. Buzzoni, E. Mucchi, G. Dalpiaz 153
Analisi vibrazionale numerica e sperimentale di un trabatto per pasta alimentare

A. Tosini, E. Mucchi, G. Dalpiaz 167
Analisi dinamica numerico-sperimentale di una motosega

A. Freddi 179
Solution of an inverse problem in the high cycle fatigue theory

B. Reggiani, L. Donati, L. Tomesani 203
Multi-cycles deformation modeling of hot forming tools under creep-fatigue regime

C. Bandini, B. Reggiani, L. Donati, L. Tomesani 221
Validazione del codice qform per l'analisi del processo di estrusione di leghe di alluminio

A. Strozzi, A. Baldini, M. Giacopini, E. Bertocchi, S. Mantovani 233
Advances in the analytical predictions of the maximum equivalent stress in a shaft-hub press-fit

D. Castagnetti, E. Dragoni 241
Un semplice modello coesivo con attrito per descrivere interfacce ibride forzate e incollate

E. Dragoni, H. F. Brinson 259
Modeling and optimization of the sandwich beam specimen in three-point bending for adhesive bond characterization

Indice degli autori 281

IMPROVEMENT OF THE DYNAMIC BEHAVIOUR OF A TEST BED DRIVELINE BY NUMERICAL AND EXPERIMENTAL INVESTIGATIONS

Marco Cocconcelli
Department of Science and Engineering Methods,
University of Modena and Reggio Emilia, Italy
E-mail: marco.cocconcelli@unimore.it

Marco Troncossi
Department of Engineering for Industry,
University of Bologna, Italy
E-mail: marco.troncossi@unibo.it

Alessandro Agazzi
Department of Engineering,
University of Ferrara, Italy
E-mail: alessandro.agazzi@unife.it

Emiliano Mucchi
Department of Engineering,
University of Ferrara, Italy
E-mail: emiliano.mucchi@unife.it

Riccardo Rubini
Department of Science and Engineering Methods,
University of Modena and Reggio Emilia, Italy
E-mail: riccardo.rubini@unimore.it

Alessandro Rivola
Department of Engineering for Industry,
University of Bologna, Italy
E-mail: alessandro.rivola@unibo.it

Giorgio Dalpiaz
Department of Engineering,
University of Ferrara, Italy
E-mail: giorgio.dalpiaz@unife.it

Abstract. *This work regards the dynamic analysis of the coupling elements in IC engine test rigs from a numerical and experimental standpoint. Two mathematical models of an IC test rig have been developed: a torsional lumped-parameter (LP) model (developed in Matlab-Simulink) for the estimation of the torsional dynamic behavior and a 3D finite element (FE) model for the estimation of the natural frequencies of the coupling elements. The numerical models take into account the stiffness and damping of the flexible elements as well as the*

test rig inertia properties. A large experimental campaign has been carried out in order to validate the models. In particular, torsional vibration measurements have been achieved by a coder-based technique using high-quality optical sensors and equidistantly spaced markers (zebra tape) on the rotating components (high flexible couplings). Eventually, the validated models have been used in order to evaluate the effect of design modifications of the coupling elements in terms of natural frequencies (torsional and bending) and torsional vibration amplitude.

Keywords: *dynamic analysis, highly flexible coupling, torsional vibration*

1. INTRODUCTION

This work addresses the dynamic analysis of the coupling elements in internal combustion (IC) engine test rigs from a numerical and experimental standpoint. In the current set up, the output shaft of the engine is connected to an electromechanical brake through a transmission shaft, which hosts an elastic coupling with rubber elements (high flexible couplings). Recently, the rising performance of engines has led to an abrupt increase of the dynamic loads affecting the driveline and in particular the elastic couplings. In this scenario, early failures of the rubber elements of the coupling have occurred.

The methodology used in order to solve the problem accounts both numerical and experimental activities. Firstly, an experimental campaign has been carried out with the aim of quantifying and characterizing the dynamic behavior of the driveline. In particular, torsional vibration measurements have been performed by a coder-based technique using high-quality optical sensors and equidistantly spaced markers (zebra tape) on the rotating components. The optical sensors were mounted before and after the coupling rubber elements, at the engine-side and brake-side, respectively.

Secondly, a 3D finite element (FE) model of the driveline has been developed in order to estimate the natural frequencies and mode shapes of the system being investigated and to evaluate which modes can negatively affect the dynamic behavior of the driveline in operational conditions. The numerical model takes into account the entire driveline with particular attention to the stiffness and inertia properties of the flexible coupling. The FE model has been experimentally validated by using data acquired during the experimental campaign mentioned above. It will be deeply discussed later on in the paper that the early failure of the elastic coupling is due to resonance phenomenon of the driveline excited at particular operational conditions. Thus, the assessed numerical model has been used in order to foresee the effect of design modifications of the coupling elements. The goal was to move the natural frequencies of the driveline outside the range of excitation of the engine harmonics.

Eventually, a lumped parameter (LP) model of the entire test rig (engine, driveline, brake) has been developed in order to estimate the torsional vibration of the system in operational conditions for the different design modifications suggested in the FE analysis. In the torsional model, developed in Matlab-Simulink environment, a precise evaluation of the variable inertia properties and torque of the engine as well as the dynamic behavior of the driveline has been included. The torsional LP model has been experimentally assessed by comparison with the experimental measurements described above. Furthermore, the torsional model enables the evaluation of the power losses in the flexible coupling in operating conditions.

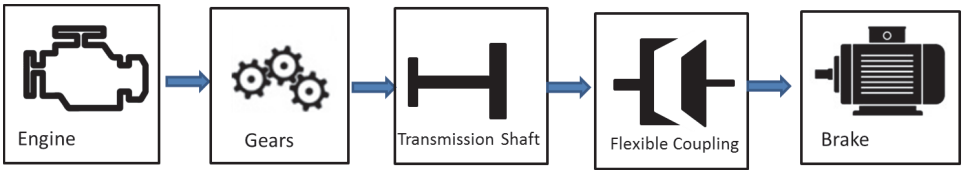

Figure 1. Schematic of the system under study.

A schematic of the test rig being studied is depicted in Fig. 1. The test rig consists of a few main components. The crankshaft of the engine drives a transmission shaft by means of the gear with a fix gear ratio. The transmission shaft is connected to the electromagnetic brake by a flexible coupling. The flexible coupling is composed of two rubber elements working in series and clumped to three metallic parts.

2. EXPERIMENTAL ANALYSIS

A brief overview of the experimental campaign is hereafter presented as well as the main results. Torsional vibration measurements have been carried out by using two optical sensors, type Optel Thevon 152 G7 GP RV4; one equipped with probe Optel Thevon MULTI TBYO 6M HM6X100 SURG and one with probe Optel Thevon MULTI SLIT YO 6M HM6X80 SURG. The zebra tape has been mounted in the two end-sections of the flexible coupling, at the brake-side and engine-side. An adequate number of lines of the zebra tape has been used in order to guarantee suitable resolution in the torsional measurement. Moreover, the tacho signal from a phonic wheel (with 8 teeth) fixed to the engine crankshaft has been acquired. The system was tested at different operational conditions, namely stationary regimes and run ups, and for different working conditions (in terms of velocity and throttle). The measured data were analyzed in the Time, Frequency, and Time-Frequency domains. Figure 2a reports the relative instantaneous angular speed (IAS) between the two end-sections of the flexible coupling during a run up of 44 s and Fig. 2b the relative Short Time Fourier Transform (STFT). The figures clearly highlight the phenomenon that determines an early failure of the coupling. In particular, in the time range between 18 and 30 seconds, the amplitude of the IAS strongly increases (Fig. 2a). The STFT clearly shows that this increase is due to a resonance of the system at about 180 Hz. The complete experimental characterization of the test rig can be found in other papers of the authors.

3. FINITE ELEMENT ANALYSIS

Model Development

An FE model (Fig. 3) has been developed in order to estimate the natural frequencies and mode shapes of the driveline. The FE model accounts the transmission shaft and the flexible coupling, which is composed of three flanges; the outer flanges allow the connections with the transmission shaft (engine-side) and with the brake, while the middle flange joins the rubber elements to the outer flanges. The engine and the brake have been included in the FE model as lumped mass elements and relative inertia (points 1 and 4 in Fig. 3): their stiffness characteristics have been neglecting. Particular attention has been devoted to the modeling of the transmission shaft and the rubber elements of the flexible coupling, since they have been identified as the most flexible components of the test rig.

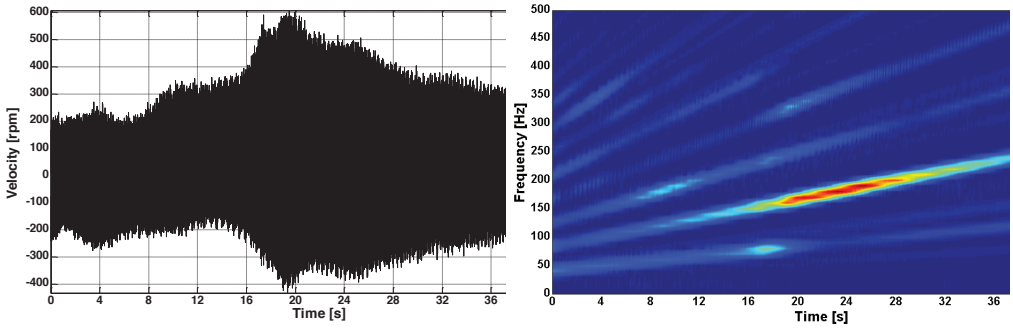

a) b)

Figure 2. Relative instantaneous angular speed between the two end-sections of the flexible coupling during a run up (a) and relative STFT (b) for the 45Sh rubber element configuration.

The flanges of the flexible coupling have been considered as lumped mass and relative inertia (points 2,3,4 in Fig. 3). Rigid links have been used in order to connect the lumped masses (the flanges, engine and brake) to the 3D meshes of the transmission shaft and rubber elements;

Table 1 collects the features of the 3D mesh. Constrains have been added (points A and B in Fig. 3) in order to represent the real boundary conditions. At the engine-side the three orthogonal displacements have been clamped while at the brake-side only the rotational coordinate θ_z has been included.

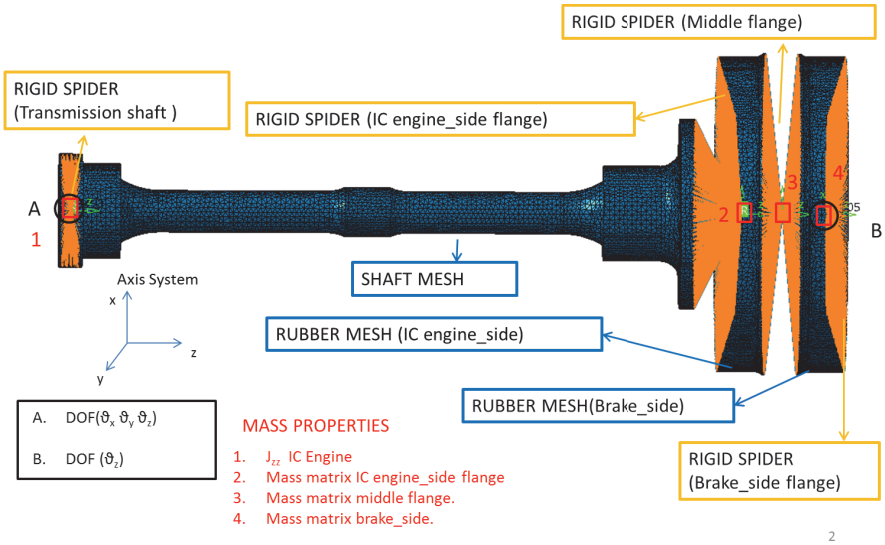

Figure 3. FE model

Figure 4. Experimental set up for estimation of rigid body inertia properties

A specific procedure has been carried out in order to evaluate the input parameters to include in the FE model. The coupling manufacturer provided the global torsional stiffness of the coupling, but the 3D FE model requires the Young's modulus of the rubber elements. Therefore, an iterative procedure based on a static FE model of the coupling has been performed in order to estimate the correct Young's modulus. A unitary torque has been applied to the FE model of the coupling and by a static analysis (MSC.Nastran SOL 101) the rotational displacement and thus the torsional stiffness have been calculated. Several simulations have been performed by changing the Young's Modulus in order to reach the torsional stiffness value provided by the manufacturer. After a few iterations, the correct Young's modulus was determined. The calculation has been repeated three times in order to find the Young's modulus for three different stiffness categories (i.e. 45Sh, 60Sh, 70Sh), as collected in Tab. 2.

The 3D-FE model requires the complete inertia tensor of the coupling flanges, while only the moment of inertia around the rotational axis was provided. In order to estimate the missing parameters, an experimental technique based on frequency response functions (FRFs) measurements (Fig. 4) has been performed for the indirect measurement of the rigid body inertia properties; such a methodology is based on the well-known Inertia Restrain Method, a technique suitable for a wide range of applications (mechanical, medical, etc [1-2]) because often the mass distribution of components or assemblies is not known. This method requires that in the FRFs, the mass line between the highest rigid body mode and the lowest flexible body mode is rather flat.

Table 2 collects the elastic properties of the rubber element estimated by the FE static analysis, the inertia properties estimated by the experimental procedure and the moment of inertia of the flanges around the rotational axis provided by the manufacturer.

Table 1. 3D meshes features

	Element type	**Number of nodes**	**Number of elements**
Transmission shaft	TETRA 4	23850	106553
Rubber element	TETRA 4	18844	80412

Model Validation

The results obtained through a numerical modal analysis (Sol 103 in MSC.Nastran) regarding 45 and 70 Shore rubber configurations have been compared with measurements (Section 2) The experimental STFT with those two rubber configurations clearly show a few resonance regions in the frequency range 0-500 Hz that are collected in Tab. 3a and Tab. 4a. Tab. 3b and Tab. 4b collect the natural frequencies estimated by the FE analysis. Regarding the 45 Shore rubber configuration, four numerical modes are very close to the resonance regions detected by the STFT. The first matching concerns the first torsional mode of the driveline, where the elements in the zone between the engine-side and the middle flange move out of phase with respect to the brake (15Hz vs 14.5Hz). The second matching regards the second torsional mode, which is characterized by a high amplitude displacement of the middle flange (70-70Hz vs 74.3Hz). Finally the last two experimental frequencies (160-190 Hz and 340Hz) correspond respectively to the 5^{th} (184.2 Hz) and the 8^{th} (348.3 Hz) numerical modes. In particular the 5^{th} numerical mode is a double mode (two roots at same frequency due to symmetry) and involved the rotation of the middle flange around axes Y and X. This is the mode mainly excited in operational conditions. The remaining modes detected in the FE analysis are not present in the experimental map, since they are not exited by the engine harmonics in operational conditions due to their particular shape. Similar considerations can be done for the 70 Sh rubber configuration (Tab. 4). The comparison between the experimental and the numerical results shows that the mode that determine the highest peaks in the experimental maps regards the third local mode of the coupling. Thus, attention should be paid in order to move this mode far away from the excitation harmonics.

4. DYNAMIC BEHAVIOR IMPROVEMENT

Experimental results have clearly shown that within the frequency band of interest (i.e. 90-300Hz, where the main excitation harmonics due to the engine lie) resonances occur.

Table 2. Input data for FE analysis. cat→from catalogue of manufacturer; exp→from experiments.

Rubber Properties	Value
Rubber Density (45-60-75 Shore)	1000 kg/m^3
Poisson's ratio	0.49
Young's modulus rubber 45 Shore (60 °C)	1.32E+06 N/m^2
Young's modulus rubber 60 Shore (60 °C)	3.11E+06 N/m^2
Young's modulus rubber 70 Shore (60 °C)	4.72E+06 N/m^2
Coupling Inertial Properties	
Mass [kg]	5.68 kg (cat)
Jxx [kgm^2]	0.01337 kgm^2 (exp)
Jyy [kgm^2]	0.01337 kgm^2 (exp)
Jzz [kgm^2]	0.01961 kgm^2 (cat)

Table 3. 45 Shore configuration. a) List of experimental resonances, b) List of simulation natural frequencies.

a)	Experimental frequencies 45 Shore	b)	Simulation results 45 Shore
Mode 1	15 Hz	**Mode 1**	14.5 Hz (First torsional mode)
		Mode 2	35.2 Hz (First local mode of coupling)
Mode 2	70 – 80 Hz	**Mode 3**	74.3 Hz (Second torsional mode)
Mode 3		**Mode 4**	98.4 Hz (Second local mode of coupling)
	160 – 190 Hz	**Mode 5**	184.2 Hz (Third local mode of coupling)
		Mode 6	220 Hz (Third torsional mode)
		Mode 7	253 Hz (Axial mode middle flange)
Mode 4	340 Hz	**Mode 8**	348.3 Hz (First bending mode output shaft)

Table 4. 70 Shore configuration. a) List of experimental resonances, b) List of simulation natural frequencies.

a)	Experimental frequencies 70 Shore	b)	Simulation results 70 Shore
Mode 1	30 – 40 Hz	**Mode 1**	25.5 Hz (First torsional mode)
		Mode 2	65.1 Hz (First local mode of coupling)
Mode 2	120 – 150 Hz	**Mode 3**	128.5 Hz (Second torsional mode)
		Mode 4	185.8 Hz (Second local mode of coupling)
		Mode 5	301 Hz (Third torsional mode)
		Mode 6	302.1 Hz (Third local mode of coupling)
		Mode 7	417.8 Hz (Axial mode middle flange)
		Mode 8	425.5 Hz (First bending mode output shaft)

Moreover, FE simulations have defined the corresponding mode shapes of such resonances. This section presents three design modifications (MOD 1, MOD 2, and MOD 3) that try to move the resonances outside the band of interest. The shifting in frequency of the resonances outside the operational bandwidth or the reduction of the number of excited modes, are the tasks for the improvement of system dynamic behavior. However, a number of design constrains should be respected as geometrical dimensions and final weight. The used methodology is as follows. The resonances close to the lower threshold of the bandwidth have been shifted below in frequency, by adding mass or reducing stiffness in specific zones, depending on the mode shape involved. The resonances close to the upper threshold have been move above in frequency by reducing mass or increasing stiffness of connection shaft and rubber elements.

Design Modification 1 – MOD 1

The first design modification (MOD 1) takes into account regards the 45Sh rubber element configuration, with increased weight of the middle flange in order to reduce the frequency of the third mode (at 89.2Hz) of the coupling; furthermore the steel connection shaft has been replaced by a stiffer titanium shaft keeping the third torsional mode outside the operational bandwidth.

Table 5. Simulation results of modified drivelines.

a)	Simulation results 45 Shore MOD 1
Mode 1	12.3 Hz (First torsional mode)
Mode 2	30.4 Hz (First local mode of coupling)
Mode 3	40 Hz (Second torsional mode)
Mode 4	69.2 Hz (Second local mode of coupling)
Mode 5	89.2 Hz (Third local mode of the coupling)
Mode 6	130.6 Hz (Axial of middle flange)
Mode 7	361 Hz (Third torsional mode)
Mode 8	493.2 Hz (First bending of output shaft)

b)	Simulation results 70 Shore MOD 2
Mode 1	22.6 Hz (First torsional mode)
Mode 2	67.1 Hz (First local mode of coupling)
Mode 3	121.6 Hz (Second torsional mode)
Mode 4	168.5 Hz (Second local mode of coupling)
Mode 5	304.3 Hz (Third local mode of coupling)
Mode 6	365.5 Hz (Axial of middle flange)
Mode 7	402.2 Hz (Third torsional mode)

c)	Simulation results 60 Shore MOD 3
Mode 1	18.7 Hz (First torsional mode)
Mode 2	57.3 Hz (First local mode of coupling)
Mode 3	124.7 Hz (Second torsional mode)
Mode 4	163.4 Hz (Second local mode of coupling)
Mode 5	310.9 Hz (Third local mode of coupling)
Mode 6	365.7 Hz (Axial of middle flange)
Mode 7	388 Hz (Third torsional mode)

Eventually, a flywheel has been introduced on the engine shaft in order to guarantee the second torsional frequency at low frequency. The comparison between Tab. 3and Tab. 5a shown that targets have been reached successfully but MOD 1 leads to a rather heavy design, which could arise issues at high-speed conditions. Therefore modifications for 70Sh configuration have been studied. Note that Mode 6 remains in the frequency range of excitation after the modification, but due to its particular shape it is not excited in operational conditions.

Design Modification 2 – MOD 2

The second design modification (MOD 2) concerns the 70Sh rubber element configuration, where the middle flange has been lightened, a flywheel on the engine shaft and a stiffer connection shaft have been placed. Table 5b collects the resulting natural frequencies. Natural frequencies still remain in the frequency range of interest, but it will be illustrated later on in Section 5, by means of the LP model, the benefits of this modification.

Design Modification 3 – MOD 3

The last design modification (MOD 3) concerns the 60 Sh rubber element configuration. The standard middle flange has been lightened by milling some parts and by replacement of steel screws with titanium ones. The transmission shaft has been included in titanium and a flywheel has been mounted on the engine shaft. Tab. 5c collects the natural frequencies. The third local mode of the coupling is above the 300Hz threshold, while the second torsional mode is still inside the operational bandwidth but the 60Sh rubber has the highest relative damping value, thus the vibration amplitude at this resonance should be reduced with respect to 70Sh. The goodness of these improvements can be appreciated also in the next section.

5. ELASTODYNAMIC ANALYSIS

Model Development

As argued in Section 3, the main dynamics effects of the coupling elements are due to the local mode of the coupling. In order to avoid these criticalities a number of design changes has been proposed in the previous section. Unfortunately the design changes are not free from possible cons in the torsional dynamics of the system. A detailed elastodynamic model is necessary to simulate the working behavior of the coupling, proving the effectiveness of suggested design corrections. Since in the frequency range of interest, after the design modifications, only torsional modes occurs (as well as a not-excited axial mode), a torsional LP model can capture the real dynamic behavior of the test rig. For these reasons the elastodynamic model of the driveline has been focused on the torsional dynamics only through a lumped parameter torsional model.

The macro physical elements of the driveline are the IC engine, the coupling, the brake and the shafts linking them to each other. Since the focus of the model is on the coupling elements, it is further divided into three main parts: the two halves facing the IC motor and the brake respectively, and the middle flange which is connected to the halves by means of rubber elements. These macro elements of the driveline are indeed the same that have been used in the FE model.

A preliminary analysis of the linking shafts inertia and stiffness suggests substituting them with a pure torsional spring of the same stiffness, while part of the inertia has been

divided between the two linked elements. The analysis is focused on the oscillations around steady working conditions only, thus the brake system will not be taken into account, i.e.. the half of the coupling facing the brake, the brake itself and the linking shaft will be considered as a fixed frame (ground). As a consequence the complexity of the mechanical system is reduced to a three degrees of freedom (DOFs) model: the torsional displacement of the IC engine (θ_1), the coupling half facing the motor (θ_2), and the middle flange of the coupling (θ_3). Figure 5 shows a schematic drawing of the 3 DOFs physical model, where J_1 is the inertia of the IC engine, J_2 of the coupling half and J_3 of the middle flange. Connections *a, b, c* refer to the transmission shaft, and the two rubber parts of the coupling, respectively. External torques acting on the single inertia are named as T_i. Note that rotational coordinates θ_1 and θ_2 correspond to the two measured locations: engine crankshaft and end-section of the coupling at the engine-side.

Inertia. Inertia J_2 and J_3 are easy to compute since they coincide with the inertia of the single mechanical parts with respect to their center of gravity, namely the half coupling and the middle flange. These values could be assumed from the FE analysis.

The computation of inertia J_1 is not trivial. It is the sum of different contributions of the internal components in the IC motor, some of them rotating with different angular speed. In order to reduce the complexity of the model, all main components – in terms of inertia – have been transported to the output axis of the motor, i.e. the one directly connected to the transmission shaft linked to the coupling. The main parts of the motors considered within inertia J_1 are:

- The alternator
- The crankshaft
- The gearboxes
- The timing system
- The clutch

Damping And Stiffness Elements. Each linking element *a, b, c* (see Fig. 5) is modeled as a spring and a viscous damper element in parallel. The resulting viscoelastic torque (T_{ve}) can be expressed as:

$$T_{ve} = k \cdot \Delta\theta + c \cdot \Delta\dot{\theta} \tag{1}$$

where k and c are the stiffness and viscous coefficient respectively, while $\Delta\theta$ and $\Delta\dot{\theta}$ are the relative rotation and relative speed of the linking element ends.

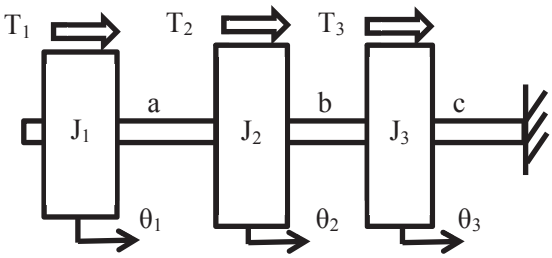

Figure 5. Schematic drawing of the physical model

Table 6. Nomenclature of the external torque parameters

Symbol	Description	Symbol	Description
P_i	Pressure in i-th cylinder	m_b	mass of the piston rod (p.r.)
d	bore of the piston	l	length of the p.r.
r	length of the crank	J_b	Inertia of the p.r.
m_p	mass of the piston	l_a	Distance COG and head of p.r.
COG	center of gravity	l_b	Distance COG and foot of p.r.

Indeed the characteristics of the transmission shaft (link *a*) are quite different from the rubber elements of the two coupling halves (links *b, c*). While the viscous damper model is correct for the steel material (in the elastic domain), for the rubber material an equivalent viscous coefficient is computed starting from an hysteretic damping model [3]. The resulting viscous coefficient is:

$$c = \frac{k \cdot \gamma}{2\pi \cdot \omega} \tag{2}$$

where γ is the relative damping value of the rubber and ω is the angular speed of the hysteretic loop. In this model ω is speed of the IC motor cycle.

External Torques. The only non-zero external torque is T_1, acting on inertia J_1 ($T_2 = T_3 = 0$). T_1 is the result of the combustion cycles of the motor in each cylinder. The torque contribution of each cylinder comes from the expansion phase in the IC cycle and the inertia momentum of each part of the crank-slide mechanism.

With reference to the nomenclature in Tab. 6 the contribution of the motor's four cylinders to the external torque gives the Eqn. (3).

$$T_1 = \sum_{i=1}^{4} \left[P_i \cdot \pi \cdot \left(\frac{d}{2}\right)^2 \cdot r_{vi} - \left(m_p + m_A - \frac{J_0}{l^2} \right) \cdot \left(\dot{\phi}_i^2 \cdot r_{ai} + \ddot{\phi}_i \cdot r_{vi} \right) \cdot r_{vi} \right] \tag{3}$$

where:

$$\begin{cases} m_A = m_b \cdot \dfrac{l_B}{l} \\ J_0 = J_b - m_b \cdot l_A \cdot l_B \\ r_{vi} = r \cdot \left(\sin\phi_i + \dfrac{1}{2} \cdot \dfrac{r}{l} \cdot \sin 2\phi_i \right) \\ r_{ai} = r \cdot \left(\cos\phi_i + \dfrac{r}{l} \cdot \cos 2\phi_i \right) \end{cases} \tag{4}$$

A detailed description of the formula in Eqn. (3) and (4) can be found in several books about the theory of machines and mechanisms, e.g [4]. Note that the quantities in Eqn. (3) and (4) without subscript index are supposed to be the same for all the cylinders, while the others differ one to each other through the combustion phase (φ_i) of each cylinder with respect to a reference (e.g. the angular displacement θ_1^* of the inertia J_1):

$$\phi_i = \theta_1^* + \varphi_i \qquad i = 1,...,4 \tag{5}$$

The superscript asterisk remembers to the reader that the angular displacement in Eqn. (5) should be the absolute displacement, not just the oscillation of inertia J_1 around the equilibrium configuration.

Equations Of Motion. The equations of (torsional) motion of the three DOFs system are computed in matrix form:

$$\begin{bmatrix} J_1 & 0 & 0 \\ 0 & J_2 & 0 \\ 0 & 0 & J_3 \end{bmatrix} \cdot \begin{bmatrix} \ddot{\theta}_1 \\ \ddot{\theta}_2 \\ \ddot{\theta}_3 \end{bmatrix} + \begin{bmatrix} c_1 & -c_1 & 0 \\ -c_1 & c_1 + c_2 & -c_2 \\ 0 & -c_2 & c_2 + c_3 \end{bmatrix} \cdot \begin{bmatrix} \dot{\theta}_1 \\ \dot{\theta}_2 \\ \dot{\theta}_3 \end{bmatrix} + \begin{bmatrix} k_1 & -k_1 & 0 \\ -k_1 & k_1 + k_2 & -k_2 \\ 0 & -k_2 & k_2 + k_3 \end{bmatrix} \cdot \begin{bmatrix} \theta_1 \\ \theta_2 \\ \theta_3 \end{bmatrix} = \begin{bmatrix} T_1 \\ 0 \\ 0 \end{bmatrix} \tag{6}$$

where c_2 and c_3 come from Eqn. (2), and T_1 from Eqn. (3). The resulting Simulink model of the test rig is shown in Fig. 6.

Model Validation

The validation of the elastodynamic model is based on the experimental analysis described in Section 2. It should be noted that experimental data collected in the 45Sh rubber element configuration cannot be used for the validation of such a model. In fact those data are mainly affected by the local mode of the coupling, which cannot be predicted by the pure-torsional model described above.

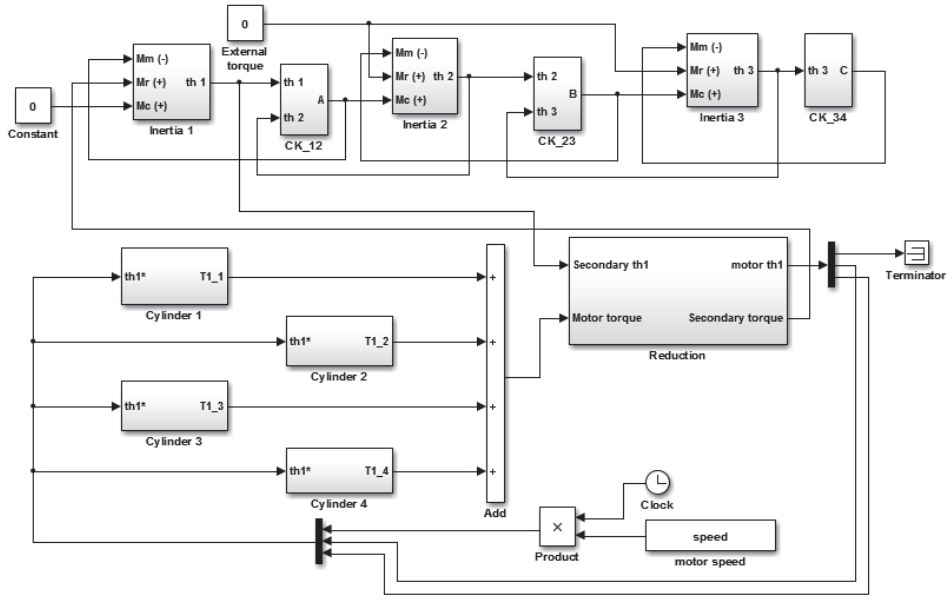

Figure 6. Simulink model of the test rig

Table 7. Comparison of resonance's frequencies in a) experimental measurements, b) FE model, c) LP model for the 70 Sh rubber element configuration

a)	Experimental resonances	b)	FE results	c)	LP results
Mode 1	30 – 40 Hz	Mode 1	25.5 Hz (1st tor.)	Mode 1	22.38 Hz
		Mode 2	65.1 Hz (1st coupl)		
Mode 2	120 – 150 Hz	Mode 3	128.5 Hz (2nd tor.)	Mode 2	124.57 Hz
		Mode 4	185.8 Hz (2nd coupl)		
		Mode 5	301 Hz (3rd tor.)	Mode 3	291.18 Hz
		Mode 6	302.1 Hz (3rd coupl.)		
		Mode 7	417.8 Hz (Axial mid)		
		Mode 8	425.5 Hz (1st bend shaft)		

The model validation is performed on data acquired in the 70 Sh rubber element configuration. As mentioned in Section 3, the coupling is available with three different types of elastic rubber elements: 45, 60 and 70 Shore of rubber hardness.

The output parameter for both experimental data and simulation results is the ratio between half the peak-to-peak and the mean value of the body oscillations, expressed as percentage. Results in correspondence of the rotational coordinates at different speed of the motor are shown in Tab. 8.

Table 8. Comparison between simulation results and experimental data

Simulation	Speed 1	Speed 2	Speed 3	Speed 4	Speed 5	Speed 6
θ_1	4.5	3.5	2.9	2.5	2.1	1.3
θ_2	4.9	2	2.2	2.7	3.0	3.4
θ_3	10.3	3.3	2.0	1.7	1.4	4.0
Experiment	**Speed 1**	**Speed 2**	**Speed 3**	**Speed 4**	**Speed 5**	**Speed 6**
θ_1	5.4	4.3	3.5	2.9	2.5	2.1
θ_2	7.9	4.0	2.9	2.4	1.8	3.2

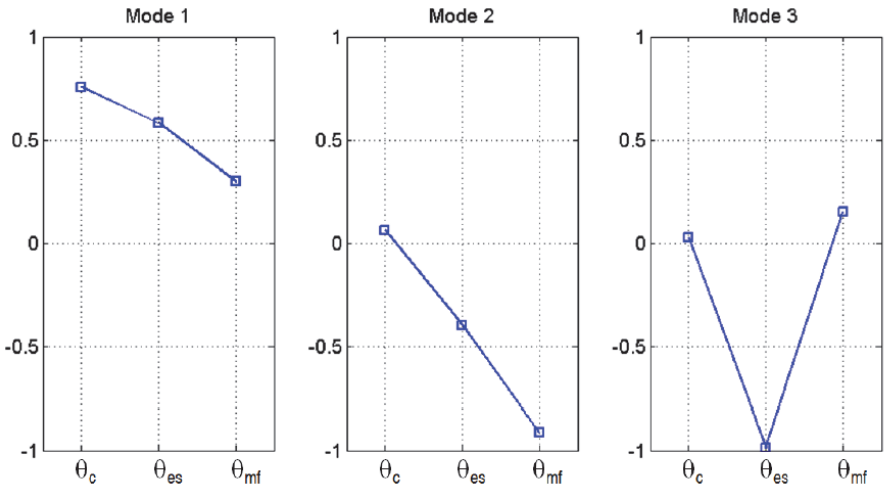

Figure 7. Normalized mode shapes of the driveline

Due to non-disclosure agreements the speed values are not present, the speed linearly increases from Speed 1 to Speed 6. θ_1, θ_2, θ_3 are three rotational coordinates. In particular θ_1 regards the oscillation of the IC motor, θ_2 the half coupling and P_3 the middle flange of the coupling. Unfortunately location $\theta_3$was not measured in the experimental analysis then it is shown for simulation results only for completeness.

Simulation results are in good accordance with the experimental data, both clearly identify a higher oscillation at Speed 1 which decreases as the speed increases from 1 to 5, and then it increases again until Speed 6. The increased oscillations at Speed 1 and 6 are confirmed also by location θ_3. The advantage of the elastodynamic model is that the causes of the increased oscillation could be easily investigated through the simulation. In particular the analysis of the resonance frequencies of the system shows that mode shape 2 is particularly burdensome for coordinate θ_3 (see Fig. 7). The corresponding natural frequency is quite close to the 1x of rotational speed 1, thus justifying both simulation results and experimental analysis. Moreover the same natural frequency is still close to the 0.5x of the rotational speed 6.

Simulation Results And Discussion

With reference to section 4 the elastodynamic model of the driveline has been used to simulate the dynamic behavior of the system after three different design changes. The same designation of the modifications discussed in section 4 is used. Results are given as the ratio between half the peak-to-peak and the mean value of the bodies oscillations, expressed as percentage – the same output parameter used in section 0.

Table 9. Simulation results of MOD 1

MOD 1	Speed 1	Speed 2	Speed 3	Speed 4	Speed 5	Speed 6
θ_1	2.4	2.1	1.8	1.3	0.9	0.7
θ_2	3.4	4.2	1.9	1.6	3.2	1.4
θ_3	0.30	0.19	0.13	0.07	0.04	0.03

Table 10. Simulation results of MOD 2

MOD 2	Speed 1	Speed 2	Speed 3	Speed 4	Speed 5	Speed 6
$\boldsymbol{\theta}_1$	2.4	2.1	1.8	1.3	1.0	0.7
$\boldsymbol{\theta}_2$	2.8	2.7	2.2	1.4	1.8	1.1
$\boldsymbol{\theta}_3$	3.24	1.55	1.14	1.04	2.09	0.35

The first design modification (MOD 1) regards 45Sh rubber elements, with increased weight of the middle flange, titanium transmission shaft and a flywheel on the engine shaft. Results are shown in Tab. 9.

The second design modification (MOD 2) concerns 70Sh rubber elements, lightened middle flange, flywheel on the engine shaft and titanium transmission shaft. Results are shown in Tab. 10.

The third design modification (MOD 3) differs from MOD 1 and MOD 2. Lighted middle flange, titanium screws, titanium connection shaft and a flywheel on the engine shaft. Results are shown in Tab. 11.

A further indicator used is the power loss. According to standard DIN 740 the relative damping is the ratio between the damping power of one vibration cycle and elastic deformation energy. The elastic deformation energy depends on the main frequency in the oscillation spectrum of the coupling and can be easily computed, while the relative damping is usually given in the manufacturer's catalog (it is the γ parameter in equation 2). The damping power of one vibration cycle for different hardness of the rubber and different speeds is collected in Tab. 12.

Modification 1 keeps torsional vibrations at low level, with a stable and limited oscillation around the reference speed. Consequently the power loss has low values compared to the other modifications. As a drawback the FE analysis shows that all the resonance frequencies are shifted to lower values, e.g. six resonances lay in the band (0-300 Hz). Even if they are outside the frequency band of interest (90 – 300 Hz), it is not excluded that the test rig will be used at lower speed regimes in the future, with the consequent need of further design modifications to avoid resonance problems again. Moreover the MOD 1 requires a sensible increase of the coupling's mass and then a further structural load on the supports of the test rig.

Modification 2 and 3 go in the opposite direction of MOD 1. They shift the resonance frequencies at higher values out of the selected frequency bandwidth. Torsional vibrations are still acceptable; the speed oscillation is less than 5% with respect to regime.

In MOD2 the FE model shows that the local mode frequency is outside the limit of 300 Hz but still close (304 Hz), while MOD 3 takes a little bit higher safety factor (311 Hz).

Table 11. Simulation results of MOD 3

MOD 3	Speed 1	Speed 2	Speed 3	Speed 4	Speed 5	Speed 6
$\boldsymbol{\theta}_1$	2.4	2.0	1.7	1.3	1.0	0.7
$\boldsymbol{\theta}_2$	2.7	4.4	2.0	1.5	4.0	1.2
$\boldsymbol{\theta}_3$	2.82	1.43	1.16	1.19	1.51	0.32

Table 12. The damping power of one vibration cycle for each design modification

[W]	Speed 1	Speed 2	Speed 3	Speed 4	Speed 5	Speed 6
MOD 1	1.03	1.23	0.72	0.99	0.98	0.87
MOD 2	31.87	13.18	4.80	4.14	2.90	1.88
MOD 3	19.14	9.76	3.83	3.54	2.66	1.89

Comparing the damping power in Tab. 12, MOD 2 shows an increased value at Speed 1 and 2 – probably due to a close resonance – which is reduced in MOD 3. These considerations lead to choose MOD 3 as the optimal design improvement.

6. CONCLUSIONS

This paper deals with the dynamic analysis of coupling elements in IC engine test rig. The test rig consists of a few main components: the engine, gears, a transmission shaft, a flexible coupling and a break. The crankshaft of the engine drives a shaft by means of the gear with a fix gear ratio. The transmission shaft is connected to the electromagnetic brake by an elastic coupling. The coupling is composed of two rubber elements working in series and clumped to three metallic parts: two halves facing the engine and the break, and a middle flange, which works as a torsional vibrations damper. Despite the peculiarity of the case study described, this paper aims to prove the complexity of a complete dynamic analysis of a mechanical system. In particular full understanding of the dynamic behavior requires more than one modeling besides an experimental activity. The first step of a dynamic analysis starts from an FE model of the system. The FE model allows the comprehension of the resonances of the system, i.e. a torsional resonances rather than a flexural or axial resonance. The experimental activity clearly shows which resonance is burdensome for the characteristic working conditions of the system, and it guides the choice of proper design modifications in order to remove critical working conditions. It must be stressed that design modifications focus on – let's call – primary dynamics effects, e.g. the flexural vibration resonance that causes an abrupt break of the system. Unfortunately the design modifications could have secondary dynamic effects, e.g. some impacts on the torsional vibrations that have not been considered yet. As a consequence the second step is the development of a lumped parameter model focused on these secondary dynamic effects, which assure the effectiveness of the design modifications in all the working conditions of the test rig. In this paper the proposed methodology is applied to the dynamic analysis of a flexible coupling. Experimental activity has shown the presence of a resonance close to the working condition of the coupling, which leads to a quickly breaking of the rubber elements of the joint. The FE model enables the characterization of the shape of the mode that determines such a resonance and the suggestion of three different design modifications to avoid the resonance in working conditions. The LP model allowed choosing the design modification less burdensome in terms of torsional vibration of the driveline.

The presented methodology could be a very useful tool in prototype design and optimization, as well as to identify the origin of unwanted dynamic effects in test rig. Although these quantitative results concern a particular test rig, the used methodology and the drawn conclusions have a general meaning from the qualitative point of view: they can be applied to a large variety of mechanical systems and applications and give useful

guidelines in order to foresee the influence of operational conditions and design modifications on vibration generation.

Acknowledgements

This work has been developed within the Advanced Mechanics Laboratory (MechLav) of Ferrara Technopole, realized through the contribution of Regione Emilia-Romagna - Assessorato Attività Produttive, Sviluppo Economico, Piano telematico – POR-FESR 2007-2013, Activity I.1.1.

REFERENCES

[1] Mucchi, E., Bottoni, G., and Di Gregorio, R., 2009. "Indirect Measurement of the Inertia Properties of a Knee Prosthesis through a Simple Frequency-Domain Technique", *Journal of Medical Devices*, **3**, December, 044501-5.

[2] Mucchi, E., Fiorati, S., Di Gregorio, R., and Dalpiaz, G., 2011, "Determining the rigid-body inertia properties of cumbersome systems: comparison of techniques in time and frequency domain", *Experimental techniques*, May/June.

[3] Rao, S.S.,2003, *Mechanical Vibrations*, Prentice Hall, New York.

[4] Uicker, J., Pennock, G., Shigley, J., 2010, *Theory of Machines and Mechanisms*, Oxford University Press, New York.

Finito di stampare
nel Luglio 2015 da
Global Print - Gorgonzola (MI)

In questo volume sono raccolte le memorie presentate in occasione della "Ottava Giornata di Studio Ettore Funaioli", che si è svolta il 18 luglio 2014 presso la Scuola di Ingegneria e Architettura dell'Alma Mater Studiorum – Università di Bologna. La Giornata è stata organizzata dagli ex allievi del Prof. Funaioli con la collaborazione del DIN – Dipartimento di Ingegneria Industriale e della Scuola di Ingegneria e Architettura dell'Alma Mater Studiorum – Università di Bologna, e con il patrocinio dell'Accademia delle Scienze dell'Istituto di Bologna e del GMA – Gruppo di Meccanica Applicata.

Questo volume è stato stampato con il contributo di G.D S.p.A.

ISBN 978-88-7488-871-9

ISBN 978-88-7488-871-9